Strong Parametric Coupling between Two Ultracoherent Membrane Modes

David Hälg,[1] Thomas Gisler,[1] Eric C. Langman,[2,3] Shobhna Misra,[1] Oded Zilberberg,[4,5] Albert Schliesser,[2,3] Christian L. Degen,[1,6] and Alexander Eichler[1,*]

[1]*Laboratory for Solid State Physics, ETH Zürich, 8093 Zürich, Switzerland*
[2]*Niels Bohr Institute, University of Copenhagen, 2100 Copenhagen, Denmark*
[3]*Center for Hybrid Quantum Networks, Niels Bohr Institute, University of Copenhagen, 2100 Copenhagen, Denmark*
[4]*Institute for Theoretical Physics, ETH Zürich, 8093 Zürich, Switzerland*
[5]*Department of Physics, University of Konstanz, D-78457 Konstanz, Germany*
[6]*Quantum Center, ETH Zurich, 8093 Zurich, Switzerland*

(Received 24 September 2021; revised 17 December 2021; accepted 3 February 2022; published 1 March 2022)

We demonstrate parametric coupling between two modes of a silicon nitride membrane. We achieve the coupling by applying an oscillating voltage to a sharp metal tip that approaches the membrane surface to within a few 100 nm. When the voltage oscillation frequency is equal to the mode frequency difference, the modes exchange energy periodically and faster than their free energy decay rate. This flexible method can potentially be useful for rapid state control and transfer between modes, and is an important step toward parametric spin sensing experiments with membrane resonators.

DOI: 10.1103/PhysRevLett.128.094301

Optomechanical resonators made from silicon nitride are a key resource for future technologies [1–8]. Owing to their very large quality factors, these devices are highly coherent and extremely sensitive to external forces [9]. They can interact with mechanical, electrical, optical, and magnetic signals, and their mechanical mode shapes and resonance frequencies can be tailored to specific situations. Promising applications of such resonators include demonstrations of fundamental light-matter interactions [10–12], gravitational-wave detection [13], quantum-coherent signal conversion between the microwave and optical domains [14,15], scanning force microscopy [9], and nanoscale magnetic resonance imaging [16,17].

One crucial ingredient for harnessing optomechanical resonators for applications involves parametric coupling, also known as parametric frequency conversion, mode locking, or three-wave mixing. This method for coupling nondegenerate modes, long-employed in electronics and nonlinear optics [18], can also be applied to nanomechanical resonators [19]. In parametric coupling, two modes with frequencies f_i and f_j are coupled through a pump tone at the frequency difference $f_p = |f_j - f_i|$. Because of the pump tone, the modes experience each other's oscillations as resonant forces, similar to coupled degenerate resonators. However, implementing efficient parametric coupling with ultracoherent optomechanical devices is difficult—the very shielding from the environment that facilitates exceptionally high quality factors [5,6] makes the implementation of a strong pump tone challenging. As a result, strong parametric coupling [20,21], where the rate of energy exchange between two nondegenerate modes exceeds their individual decay rates, has so far not been demonstrated with ultrahigh Q resonators.

In this Letter, we demonstrate strong parametric coupling between two shielded mechanical modes in a silicon nitride membrane. We circumvent the shielding issue with a sharp metallic tip that approaches the membrane to a few 100 nm, enabling local and precise control of the electrical interaction force gradient. With this control, we demonstrate parametric coupling with a time $t_\Delta = 4.8$ s required to transmit energy from one mode to the other and back, roughly 7 times faster than the mechanical decay time τ. Our method can be further improved by increasing the power delivered by the electrical pump tone, the electrical makeup of the membrane surface, and the quality factor of the mechanical modes, leading ultimately to quantum coherent state transfer between nondegenerate modes.

At the heart of our experiment is a silicon nitride membrane resonator whose displacement is detected with a power-balanced laser interferometer at 1550 nm; see Fig. 1(a). The time-dependent light intensity is transformed into an electrical signal and measured with a Zurich Instruments HF2LI lock-in amplifier. A sharp (rigid) metal tip can be scanned over the membrane surface with a three-axis stage [9]. The 20 nm–thick membrane features a hole pattern that implements a phononic crystal [5]. Two "lotus" defect [22] islands in the pattern with a separation of roughly 1.2 mm and with quality factors $Q = 1.4 \times 10^8$ act as isolated resonators 1 and 2. The symmetric (S) and antisymmetric (A) normal modes of these resonators, shown in Fig. 1(b), extend over both defect sites and have an effective mass m of around 6.9 ng [23]. In the spectra in Figs. 1(c) and 1(d), the normal modes appear as narrow lines at frequencies $f_{A,S}$ inside the band gap created by the phononic crystal. To achieve these high quality factors, the

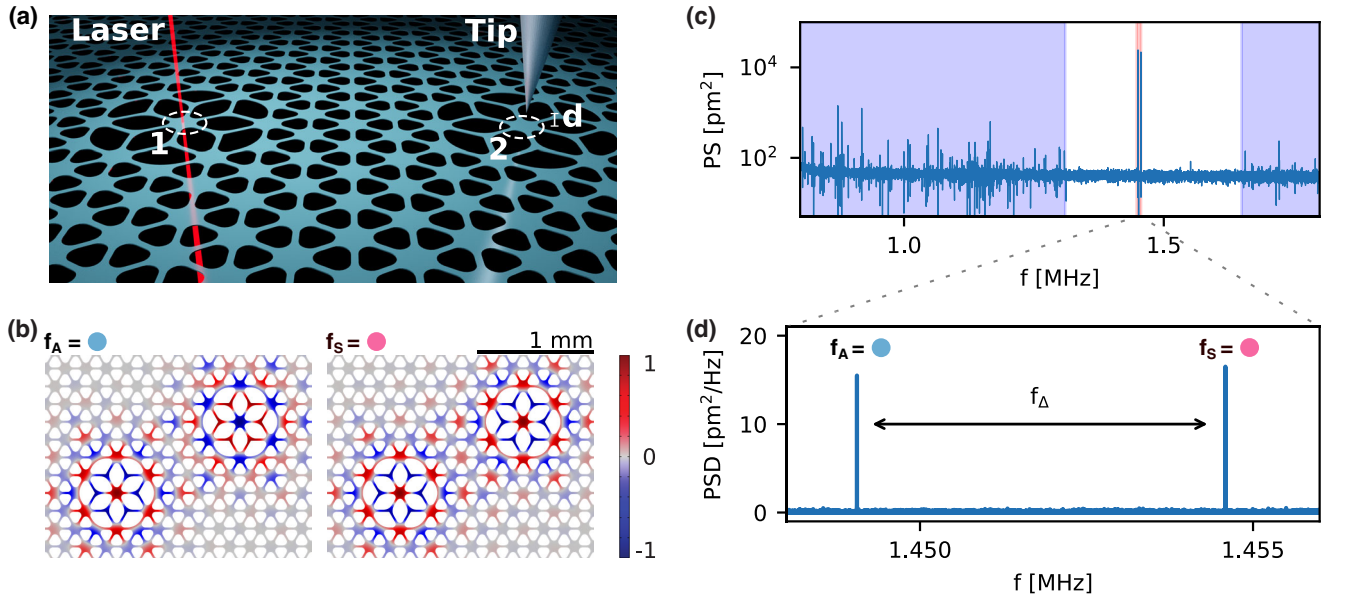

FIG. 1. Setup and characterization. (a) Sketch of the setup, showing the phononic crystal hole pattern with two defect sites labeled 1 and 2. The interferometric readout and driving lasers are centered on defect site 1 and the scanning tip is centered at a distance d above defect 2. (b) Simulated displacement of the antisymmetric (left) and symmetric (right) membrane modes in arbitrary units. (c) Displacement power spectrum obtained by slowly sweeping the frequency of the laser drive. Shaded blue region: modes outside of the band gap. Shaded red region: frequency range shown in (d). (d) Displacement power spectral density of the membrane modes shown in (b), driven by thermomechanical force noise. The left and right peaks are the antisymmetric and symmetric modes, respectively, color coded in light blue and pink throughout the Letter.

experiment is placed in a vacuum chamber at around 1×10^{-7} mbar and thermally stabilized at a temperature of 30 °C.

We can apply resonant driving forces to the two modes and measure their oscillatory response; see Fig. 2. First, we drive mode A with the photon pressure of a 980 nm laser whose intensity I_{laser} is modulated at $f_d = f_A$ [9], generating a force $F_A \propto I_{\text{laser}}$. Second, we drive the same mode by modulating the voltage applied to the scanning tip as $V_{\text{tip}} = V_{\text{AC}} \cos(2\pi f_d t)$ [9]. The response for $f_d = f_A$

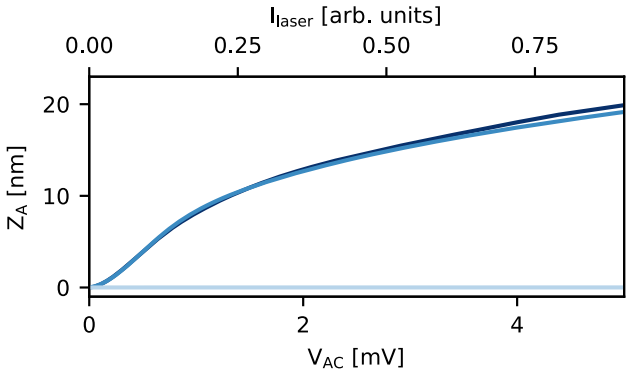

FIG. 2. Comparison of different driving methods. The amplitude Z_A of the antisymmetric mode driven with a photon pressure modulated at $f_d = f_A$ (dark blue), with a voltage applied to the tip at $f_d = f_A$ (medium blue) and with a tip voltage at $f_d = \frac{1}{2} f_A$ (light blue).

exhibits the same nonlinear saturation at large amplitudes as obtained with the photon drive. There are three possibilities for how an electrical force can arise: (i) for a conducting sample, a Coulomb force is generated between the charged tip and mirror charges on the membrane surface. Since our membrane is made from a dielectric, we think this to be an unlikely option. (ii) The dielectric membrane material can become polarized in response to the applied voltage [24]. For both (i) and (ii), we expect $F_A \propto V_{\text{AC}}^2$ and that the force appears at $2f_d$ instead of f_d. However, our measurements indicate $F_A \propto V_{\text{AC}}$ and the vibrational response when driving at $f_d = f_A/2$, shown in Fig. 2 for comparison, is negligible. (iii) We finally propose that the force is caused by the interaction of the tip with "voltage patches" on the membrane surface [25–31]. A similar interaction was recently observed with a different nanomechanical system [32]. This model can qualitatively explain all phenomena in Figs. 2–4. Additional data in the Supplemental Material [33] support this interpretation.

Our system can be modeled with a set of coupled equations of the form

$$\ddot{z}_A + \omega_A^2 z_A + \Gamma_A \dot{z}_A - J z_S = F_A/m_A \tag{1a}$$

$$\ddot{z}_S + \omega_S^2 z_S + \Gamma_S \dot{z}_S - J z_A = F_S/m_S. \tag{1b}$$

Here, z_i is the displacement (with dots signifying time derivatives), $\omega_i = 2\pi f_i$ the angular resonance frequency,

$\Gamma = (\omega_i/Q_i)$ the dissipation coefficient of mode i with quality factor Q_i, m_i the effective mass, and F_i the force acting on mode i. For perfectly degenerate defect resonators 1 and 2, the normal modes S and A are fully decoupled. Finite detuning between the defect resonators, in contrast, leads to finite coupling J [40]. Consequently, a modulation of the detuning between the resonators at a frequency f_p, which is chosen to be equal to $f_\Delta = f_S - f_A$ or $f_\Sigma = f_S + f_A$, leads to a coupling term $Jz_j = 2\omega_0 g\cos(2\pi f_p t)z_j$ that has a component that is resonant with f_i, with $\omega_0 = (\omega_S + \omega_A)/2$ [17,40]. This "parametric coupling" can be used for an efficient energy exchange between modes at very different frequencies [19,20,41] and represents a bosonic, classical analog to Rabi oscillations.

We derive a formal description of the parametric coupling process via the averaging method [33]. In a frame rotating at $f_i^{\mathrm{av}} \approx f_i$, the displacement z_i can be expressed in terms of in-phase and out-of-phase oscillation amplitudes u_i and v_i, respectively. The time evolution of the system is then obtained from the coupled slow-flow equations

$$\begin{bmatrix} \dot{u}_S \\ \dot{v}_S \\ \dot{u}_A \\ \dot{v}_A \end{bmatrix} = \frac{1}{2}\begin{bmatrix} -\Gamma & 2\delta_S & 0 & \sigma g \\ -2\delta_S & -\Gamma & -g & 0 \\ 0 & \sigma g & -\Gamma & 2\delta_A \\ -g & 0 & -2\delta_A & -\Gamma \end{bmatrix}\begin{bmatrix} u_S \\ v_S \\ u_A \\ v_A \end{bmatrix} + \begin{bmatrix} 0 \\ \frac{-F_S}{2m\omega_0} \\ 0 \\ \frac{-F_A}{2m\omega_0} \end{bmatrix}, \tag{2}$$

where $\delta_i/2\pi = f_i^{\mathrm{av}} - f_i$ are small detunings from the ideal rotating frame, and we use the notation $\sigma = 1$ ($\sigma = -1$) for driving at $f_p = f_\Delta$ ($f_p = f_\Sigma$). Our choice of zero phase offset for F_A and F_S leads to force terms that act solely on the v_A and v_S coordinates on resonance. The result we obtain for pumping at $f_p = f_\Delta$ is identical to the one previously derived with a different method [40]. Below, we concentrate on results obtained by driving at f_Δ. We refer the reader to the Supplemental Material for an example of driving at f_Σ [33].

A time-dependent detuning J between the resonators 1 and 2 is achieved by applying an electrical drive tone $V_{\mathrm{tip}} = V_{\mathrm{AC}}\cos(2\pi f_p t)$ to resonator 2 via the scanning tip. The corresponding force gradient gives rise to an electrical spring constant $k_{\mathrm{el}}(t) = -[dF_{\mathrm{el}}(t)/dz]$ that modifies the resonator's resonance frequency f_2 as a function of time. This detuning effectively couples the normal modes with a coefficient $J = k_{\mathrm{el}}/m$ [33,40].

In Fig. 3, we experimentally investigate parametric coupling at $f_p = f_\Delta$ in the absence of an external force. In Fig. 3(a), the antisymmetric mode is initially driven to high amplitude by a resonant laser drive. The laser drive is then switched off and a parametric pump tone at f_Δ is switched on. The two modes exchange energy periodically in additional to an overall ringdown. The theoretical fit yields a coupling frequency of $g = (2\pi/t_\Delta) = 1.3\ \mathrm{rad\,s^{-1}}$,

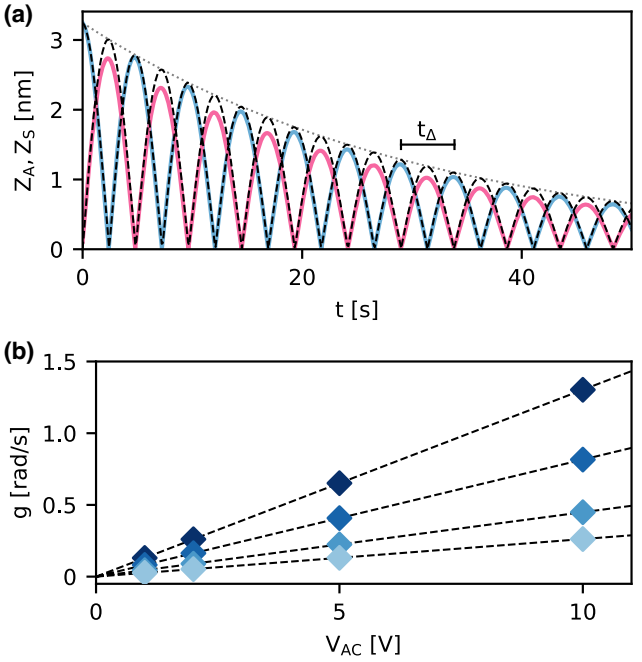

FIG. 3. Parametric pumping at f_Δ. (a) Parametric pumping with $V_{\mathrm{AC}} = 10$ V at $d = 100$ nm and with initial conditions $Z_S(0) = 0$, $Z_A(0) = 3.25$ nm. Blue and pink: measured amplitudes $Z_i = \sqrt{u_i^2 + v_i^2}$ of the antisymmetric and symmetric modes, respectively. Black dashed line: theory fit using Eq. (2) with $g = 1.3\ \mathrm{rad\,s^{-1}}$ and $\delta_{S,A} = 0$. Gray dotted line: exponential decay with the average of the ringdown times $\tau_i = Q_i/\pi f_i$. (b) Coupling strength g versus tip voltage. From light to dark blue at each voltage: $d = 1000$ nm, 500 nm, 200 nm, and 100 nm. Dashed lines are linear fits.

which is the highest coupling frequency we achieved with this device (for $V_{\mathrm{AC}} = 10$ V and $d = 100$ nm). In Fig. 3(b), we collect the measured values of g for different V_{AC} and d. We find a linear dependence on V_{AC}, while the increase in coupling frequency is stronger than linear with d.

When applying a resonant laser (photon pressure) drive to mode A and a parametric pump tone at f_Δ simultaneously, the system reaches an out-of-equilibrium steady state after a time $t \gg Q/\pi f$ [17,19]. The amplitudes of this steady state depend on $V_{\mathrm{AC}} \propto g$, offering an alternative way to measure the coupling. The measured and calculated results are shown in Fig. 4(a). For increasing parametric coupling, the steady-state amplitudes begin to equalize and cross at $\approx$2.5 V, whereafter mode A has the *smaller* amplitude of the two modes. To understand this, we need to remember that the phase of mode S follows the force exerted by the coupling term with a phase lag of $-\pi/2$, and that mode S in turn drives mode A with a second phase lag of $-\pi/2$. In total, mode A damps itself through this feedback loop, and its amplitude follows the simple closed form (see the Supplemental Material [33])

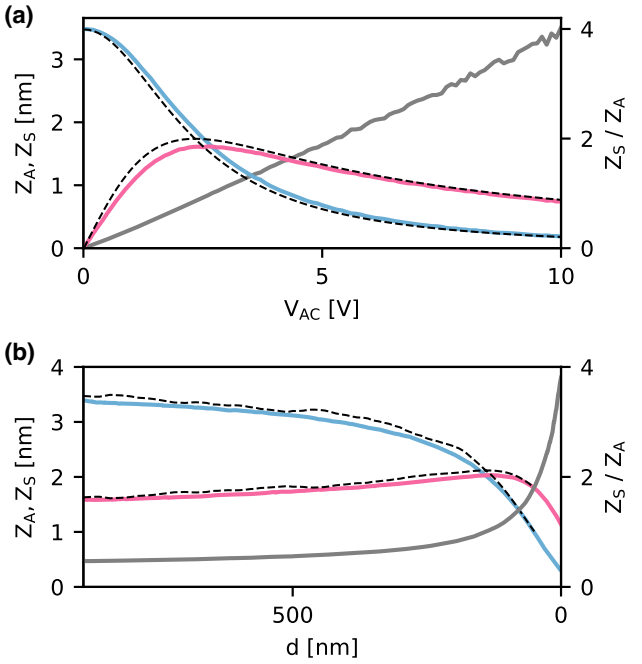

FIG. 4. Steady-state amplitudes. (a) Mode amplitudes as a function of V_{AC} with a constant photon pressure drive at $f_d = f_A$ and parametric pumping at f_Δ at a distance $d = 1000$ nm (left axis). Blue and pink: measured amplitude of the antisymmetric and symmetric modes, respectively. Black dashed lines: solutions of Eq. (2) for $\dot{u}_{S,A} = \dot{v}_{S,A} = 0$. (b) Mode amplitudes as a function of d with $V_{\mathrm{AC}} = 1$ V. Black dashed lines: solutions of Eq. (2), a finite-element numerical charge distribution model; see the Supplemental Material [33]. Gray lines and right axes: Z_S/Z_A extracted from the measurements.

$$Z_A = \sqrt{u_A^2 + v_A^2} = -i\frac{F_A}{m\omega_0\Gamma}\left[1 + \left(\frac{g}{\Gamma}\right)^2\right]^{-1}, \quad (3)$$

while the ratio between the two amplitudes is

$$\frac{Z_S}{Z_A} = -i\frac{g}{\Gamma}. \quad (4)$$

We find excellent correspondence between the measurements and Eqs. (3) and (4), using F_A and g as free parameters. The value $g = 0.25$ rad s^{-1} obtained for $V_{AC} = 10$ V and $d = 1000$ nm is the same (within fit errors) as the one we found for identical conditions in Fig. 3. For fixed V_{AC}, we can increase the coupling g by reducing d; see Fig. 4(b). To model these data, we simulate the tip field and the interaction with a surface charge distribution in COMSOL. We heuristically find a surface charge distribution that fits the measured $g(d)$; cf. the Supplement Material [33].

The agreement between experiment and theory serves as a foundation for future applications. In particular, the linear relationship between the two mode amplitudes in Fig. 4(a) is an important "dress rehearsal" for nuclear spin detection with a membrane resonator [17]. In this proposal, the parametric pumping is provided by an ensemble of periodically inverted nuclear spins, whose number can then be estimated from the amplitude of the undriven mode (Z_S in Fig. 4). Our experiment shows that the parametric energy exchange between modes follows a simple mathematical form and is not significantly affected by the modes' nonlinearities [17,23] in the studied amplitude range.

Parametric mode conversion can also be of potential use for purely electrical applications of scanning force microscopy. For instance, a deeper understanding of the microscopic origin of mechanical damping will require highly resolved and ultrasensitive imaging of trapped charges on resonator surfaces [25–32]. For a single charge, the force sensitivity of the parametric frequency conversion method (cf. Fig. 4) can be compared to the direct-drive method, which we illustrate here with a simplified example. Direct driving between a single surface charge q_{surf} and a spherical tip with a charge q_{tip} results in the Coulomb force

$$F_S = \frac{1}{4\pi\epsilon_0}\frac{q_{\mathrm{tip}}q_{\mathrm{surf}}}{(d+R)^2}, \quad (5)$$

where ϵ_0 is the permittivity of free space and $d + R$ the separation between the effective charge positions, with R the tip radius. The force is the first derivative of the resonator's electric potential E_c in the presence of a charged tip. In contrast, the parametric method probes the second derivative of E_c and yields

$$F_{\mathrm{par}} = Jz_A = -\frac{1}{2\pi\epsilon_0}\frac{q_{\mathrm{tip}}q_{\mathrm{surf}}}{(d+R)^3}z_A. \quad (6)$$

The two forces become equal for $z_A = (d + R)/2$, which can in principle be attained for $d > R$. Note that the electric force in Eq. (5) and its derivative in Eq. (6) may differ for a realistic tip geometry. Nevertheless, we expect that both methods will generally yield good signals. Inserting into Eq. (6) the numerical values $q_{\mathrm{tip}} = q_{\mathrm{surf}} = 0.16$ aC (one elementary charge), $d = R = 50$ nm, and $z_S = 10$ nm, we obtain $F_{\mathrm{par}} = 4.6$ fN. This force should be routinely detected with our ultrasensitive membrane resonators whose force noise will drop below 1 aNZ$^{-1/2}$ at cryogenic temperatures [9]. Significantly higher forces can be generated by increasing the tip charge—for the self-capacitance $C_{\mathrm{self}} = 4\pi\epsilon_0 R$ of a sphere with radius $R = 50$ nm, a tip voltage $V_{\mathrm{tip}} = 10$ V induces 350 elementary charges. We propose to implement the direct and parametric methods simultaneously to gain access to complementary information, i.e., the first and second derivatives of the tip-surface interaction energy, to improve the determination of the electrical fields.

To conclude, we have demonstrated strong (classical) parametric coupling between two membrane modes induced by the time-dependent voltage on a scanning

tip. This achievement unlocks a large toolbox that vastly increases the range of possible experiments using such resonators. First, strong mode coupling was shown to be a useful way to avoid long transient dynamics and to obtain rapid resonator control [42]. Second, our experiment serves an electrical test for parametric spin sensing experiments that will couple two resonator modes via coherently inverted nuclear spins [17,19]. Third, our study motivates additional investigations of the membrane's electrical surface states, allowing deeper insights into the surface chemistry and the microscopic nature of noncontact friction [9,32,43]. Finally, with further improvements of the parametric coupling strength g, we could accomplish quantum-coherent state transfer between nondegenerate modes. Similarly, when combined with optomechanical techniques that remove entropy, the techniques presented here can enable quantum squeezing and entanglement of the mechanical modes [44,45], which can enhance the sensitivity in the measurement of small forces [46,47]. The best dissipation-limited quantum coherence times for membrane resonators are on the order of milliseconds at 4 K [11] and already exceed 100 ms at dilution refrigerator temperatures [22]. This means that our experimental approach requires only a moderate improvement to overcome the decoherence stemming from dissipation, while decoherence caused by frequency noise is currently not well characterized in this system. Our scanning probe–based approach is, in addition, very flexible with regard to different modes of vibration, whose optimal coupling points (in real space) are located at different positions.

We gratefully acknowledge technical support by the mechanical workshop of D-PHYS at ETH Zurich. This work was supported by Swiss National Science Foundation (SNSF) through the National Center of Competence in Research in Quantum Science and Technology (NCCR QSIT), the Sinergia grant (CRSII5_177198/1), and the project Grant 200020-178863, Danmarks Grundforskningsfond (DNRF) Center of Excellence Hy-Q, the European Research Council through the ERC Starting Grant Q-CEOM (Grant Agreement 638765), and the ERC Consolidator grant PHOQS (Grant Agreement 101002179), the DFG Heisenberg grant, as well as an ETH research grant (ETH-03 16-1).

*Corresponding author.
eichlera@ethz.ch

[1] S. S. Verbridge, H. G. Craighead, and J. M. Parpia, A megahertz nanomechanical resonator with room temperature quality factor over a million, Appl. Phys. Lett. **92**, 013112 (2008).

[2] G. Anetsberger, E. Gavartin, O. Arcizet, Q. P. Unterreithmeier, E. M. Weig, M. L. Gorodetsky, J. P. Kotthaus, and T. J. Kippenberg, Measuring nanomechanical motion with an imprecision below the standard quantum limit, Phys. Rev. A **82**, 061804(R) (2010).

[3] C. Reetz, R. Fischer, G. G. T. Assumpção, D. P. McNally, P. S. Burns, J. C. Sankey, and C. A. Regal, Analysis of Membrane Phononic Crystals with Wide Band Gaps and Low-Mass Defects, Phys. Rev. Applied **12**, 044027 (2019).

[4] C. Reinhardt, T. Müller, A. Bourassa, and J. C. Sankey, Ultralow-Noise Sin Trampoline Resonators for Sensing and Optomechanics, Phys. Rev. X **6**, 021001 (2016).

[5] Y. Tsaturyan, A. Barg, E. S. Polzik, and A. Schliesser, Ultracoherent nanomechanical resonators via soft clamping and dissipation dilution, Nat. Nanotechnol. **12**, 776 (2017).

[6] A. H. Ghadimi, S. A. Fedorov, N. J. Engelsen, M. J. Bereyhi, R. Schilling, D. J. Wilson, and T. J. Kippenberg, Elastic strain engineering for ultralow mechanical dissipation, Science **360**, 764 (2018).

[7] A. Beccari, M. J. Bereyhi, R. Groth, S. A. Fedorov, A. Arabmoheghi, N. J. Engelsen, and T. J. Kippenberg, Hierarchical tensile structures with ultralow mechanical dissipation, arXiv:2103.09785.

[8] A. Beccari, D. A. Visani, S. A. Fedorov, M. J. Bereyhi, V. Boureau, N. J. Engelsen, and T. J. Kippenberg, Strained crystalline nanomechanical resonators with ultralow dissipation, arXiv:2107.02124.

[9] D. Hälg, T. Gisler, Y. Tsaturyan, L. Catalini, U. Grob, M.-D. Krass, M. Héritier, H. Mattiat, A.-K. Thamm, R. Schirhagl, E. C. Langman, A. Schliesser, C. L. Degen, and A. Eichler, Membrane-Based Scanning Force Microscopy, Phys. Rev. Applied **15**, L021001 (2021).

[10] R. W. Peterson, T. P. Purdy, N. S. Kampel, R. W. Andrews, P.-L. Yu, K. W. Lehnert, and C. A. Regal, Laser Cooling of a Micromechanical Membrane to the Quantum Backaction Limit, Phys. Rev. Lett. **116**, 063601 (2016).

[11] M. Rossi, D. Mason, J. Chen, Y. Tsaturyan, and A. Schliesser, Measurement-based quantum control of mechanical motion, Nature (London) **563**, 53 (2018).

[12] D. Mason, J. Chen, M. Rossi, Y. Tsaturyan, and A. Schliesser, Continuous force and displacement measurement below the standard quantum limit, Nat. Phys. **15**, 745 (2019).

[13] M. A. Page, M. Goryachev, H. Miao, Y. Chen, Y. Ma, D. Mason, M. Rossi, C. D. Blair, L. Ju, D. G. Blair, A. Schliesser, M. E. Tobar, and C. Zhao, Gravitational wave detectors with broadband high frequency sensitivity, Commun. Phys. **4** (2021).

[14] T. Bagci, A. Simonsen, S. Schmid, L. G. Villanueva, E. Zeuthen, J. Appel, J. M. Taylor, A. Sørensen, K. Usami, A. Schliesser, and E. S. Polzik, Optical detection of radio waves through a nanomechanical transducer, Nature (London) **507**, 81 (2014).

[15] R. W. Andrews, R. W. Peterson, T. P. Purdy, K. Cicak, R. W. Simmonds, C. A. Regal, and K. W. Lehnert, Bidirectional and efficient conversion between microwave and optical light, Nat. Phys. **10**, 321 (2014).

[16] R. Fischer, D. P. McNally, C. Reetz, G. G. T. Assumpção, T. Knief, Y. Lin, and C. A. Regal, Spin detection with a micromechanical trampoline: Towards magnetic resonance microscopy harnessing cavity optomechanics, New J. Phys. **21**, 043049 (2019).

[17] J. Košata, O. Zilberberg, C. L. Degen, R. Chitra, and A. Eichler, Spin Detection via Parametric Frequency Conversion in a Membrane Resonator, Phys. Rev. Applied **14**, 014042 (2020).
[18] R. W. Boyd, *Nonlinear Optics* (Academic Press, New York, 2020).
[19] W. M. Dougherty, K. J. Bruland, J. L. Garbini, and J. A. Sidles, Detection of AC magnetic signals by parametric mode coupling in a mechanical oscillator, Meas. Sci. Technol. **7**, 1733 (1996).
[20] T. Faust, J. Rieger, M. J. Seitner, J. P. Kotthaus, and E. M. Weig, Coherent control of a classical nanomechanical two-level system, Nat. Phys. **9**, 485 (2013).
[21] H. Okamoto, A. Gourgout, C.-Y. Chang, K. Onomitsu, I. Mahboob, E. Y. Chang, and H. Yamaguchi, Coherent phonon manipulation in coupled mechanical resonators, Nat. Phys. **9**, 480 (2013).
[22] Y. Seis, T. Capelle, E. Langman, S. Saarinen, E. Planz, and A. Schliesser, Ground state cooling of an ultracoherent electromechanical system, arXiv:2107.05552.
[23] L. Catalini, Y. Tsaturyan, and A. Schliesser, Soft-Clamped Phononic Dimers for Mechanical Sensing and Transduction, Phys. Rev. Applied **14**, 014041 (2020).
[24] Q. P. Unterreithmeier, E. M. Weig, and J. P. Kotthaus, Universal transduction scheme for nanomechanical systems based on dielectric forces, Nature (London) **458**, 1001 (2009).
[25] J. B. Camp, T. W. Darling, and R. E. Brown, Macroscopic variations of surface potentials of conductors, J. Appl. Phys. **69**, 7126 (1991).
[26] N. A. Burnham, R. J. Colton, and H. M. Pollock, Work-Function Anisotropies as an Origin of Long-Range Surface Forces, Phys. Rev. Lett. **69**, 144 (1992).
[27] F. Rossi and G. I. Opat, Observations of the effects of adsorbates on patch potentials, J. Phys. D **25**, 1349 (1992).
[28] C. C. Speake and C. Trenkel, Forces between Conducting Surfaces due to Spatial Variations of Surface Potential, Phys. Rev. Lett. **90**, 160403 (2003).
[29] N. Gaillard, M. Gros-Jean, D. Mariolle, F. Bertin, and A. Bsiesy, Method to assess the grain crystallographic orientation with a submicronic spatial resolution using kelvin probe force microscope, Appl. Phys. Lett. **89**, 154101 (2006).
[30] N. A. Robertson, J. R. Blackwood, S. Buchman, R. L. Byer, J. Camp, D. Gill, J. Hanson, S. Williams, and P. Zhou, Kelvin probe measurements: Investigations of the patch effect with applications to ST-7 and LISA, Classical Quantum Gravity **23**, 2665 (2006).
[31] J. Zúñiga-Pérez, V. Muñoz-Sanjosé, E. Palacios-Lidón, and J. Colchero, Polarity Effects on ZnO Films Grown Along the Nonpolar $[11\bar{2}0]$ Direction, Phys. Rev. Lett. **95**, 226105 (2005).
[32] M. Héritier, R. Pachlatko, Y. Tao, J. M. Abendroth, C. L. Degen, and A. Eichler, Spatially resolved surface dissipation over metal and dielectric substrates, Phys. Rev. Lett. **127**, 216101 (2021).
[33] See Supplemental Material, which includes [34–39], at http://link.aps.org/supplemental/10.1103/PhysRevLett.128.094301 for additional discussions on the surface charge, the data from a second device, the derivation of the coupling process, and the driving at the frequency sum.
[34] J. Moser, A. Eichler, J. Güttinger, M. I. Dykman, and A. Bachtold, Nanotube mechanical resonators with quality factors of up to 5 million, Nat. Nanotechnol. **9**, 1007 (2014).
[35] J. Košata, J. del Pino, T. L. Heugel, and O. Zilberberg, HarmonicBalance.jl: A Julia suite for nonlinear dynamics using harmonic balance, arXiv:2202.00571.
[36] L. Papariello, O. Zilberberg, A. Eichler, and R. Chitra, Ultrasensitive hysteretic force sensing with parametric nonlinear oscillators, Phys. Rev. E **94**, 022201 (2016).
[37] A. Olkhovets, D. W. Carr, J. M. Parpia, and H. G. Craighead, Non-degenerate nanomechanical parametric amplifier, in *14th IEEE International Conference on Micro Electro Mechanical Systems, MEMS 2001 (Cat. No.01CH37090)*, Technical Digest (IEEE, Interlaken, 2001), pp. 298–300.
[38] W. Zhang, R. Baskaran, and K. L. Turner, Effect of cubic nonlinearity on auto-parametrically amplified resonant {MEMS} mass sensor, Sens. Actuators A **102**, 139 (2002).
[39] R. Lifshitz and M. C. Cross, Nonlinear dynamics of nanomechanical and micromechanical resonators, in *Reviews of Nonlinear Dynamics and Complexity*, edited by H. G. Schuster (Wiley-VCH Verlag GmbH & Co. KGaA, New York, 2008), p. 152.
[40] M. Frimmer and L. Novotny, The classical bloch equations, Am. J. Phys. **82**, 947 (2014).
[41] H. Okamoto, A. Gourgout, C.-Y. Chang, K. Onomitsu, I. Mahboob, E. Y. Chang, and H. Yamaguchi, Coherent phonon manipulation in coupled mechanical resonators, Nat. Phys. **9**, 480 (2013).
[42] H. Okamoto, I. Mahboob, K. Onomitsu, and H. Yamaguchi, Rapid switching in high-q mechanical resonators, Appl. Phys. Lett. **105**, 083114 (2014).
[43] S. M. Yazdanian, J. A. Marohn, and R. F. Loring, Dielectric fluctuations in force microscopy: Noncontact friction and frequency jitter, J. Chem. Phys. **128**, 224706 (2008).
[44] A. Szorkovszky, A. A. Clerk, A. C. Doherty, and W. P. Bowen, Mechanical entanglement via detuned parametric amplification, New J. Phys. **16**, 063043 (2014).
[45] M. Wang, X.-Y. Lü, Y.-D. Wang, J. Q. You, and Y. Wu, Macroscopic quantum entanglement in modulated optomechanics, Phys. Rev. A **94**, 053807 (2016).
[46] S. Burd, R. Srinivas, J. Bollinger, A. Wilson, D. Wineland, D. Leibfried, D. Slichter, and D. Allcock, Quantum amplification of mechanical oscillator motion, Science **364**, 1163 (2019).
[47] S. Kotler, G. A. Peterson, E. Shojaee, F. Lecocq, K. Cicak, A. Kwiatkowski, S. Geller, S. Glancy, E. Knill, R. W. Simmonds *et al.*, Direct observation of deterministic macroscopic entanglement, Science **372**, 622 (2021).